UNIVERSITÀ DI PARMA
ARCHIVIO DELLA RICERCA

University of Parma Research Repository

A numerical study of the use of C-V characteristics to extract the doping density of CIGS absorbers

This is the peer reviewd version of the followng article:

Original
A numerical study of the use of C-V characteristics to extract the doping density of CIGS absorbers / Sozzi, Giovanna; Lazzarini, M.; Menozzi, Roberto; Carron, R.; Avancini, E.; Bissig, B.; Buecheler, S.; Tiwari, A. N.. - ELETTRONICO. - (2016), pp. 2283-2288. (Intervento presentato al convegno 43rd IEEE Photovoltaic Specialists Conference, PVSC 2016 tenutosi a Portland, OR, USA nel 5-10 June 2016) [10.1109/PVSC.2016.7750043].

Availability:
This version is available at: 11381/2821206 since: 2017-09-06T15:00:32Z

Publisher:
IEEE

Published
DOI:10.1109/PVSC.2016.7750043

Terms of use:

Anyone can freely access the full text of works made available as "Open Access". Works made available

Publisher copyright

note finali coverpage

(Article begins on next page)

15 May 2024

A numerical study of the use of C-V characteristics to extract the doping density of CIGS absorbers

G. Sozzi[1], M. Lazzarini[1], R. Menozzi[1], R. Carron[2], E. Avancini[2], B. Bissig[2], S. Buecheler[2], A. N. Tiwari[2]

[1] Department of Information Engineering - University of Parma
Parco Area delle Scienze 181A, 43124 Parma, Italy

[2] Laboratory for Thin Films and Photovoltaics, Empa - Swiss Federal Laboratories for Materials Science and Technology, Ueberlandstrasse 129, CH-8600 Duebendorf, Switzerland.

***Abstract* - In this work we use numerical simulations to study how the doping profile extracted by the commonly used C-V technique is influenced by the solar cell main features, as the doping and thickness of different layers, or the conduction band offsets at hero-interfaces. The doping profiles dependence on temperature is also investigated. The effect of both acceptor and donor deep defects of different energy and density on the simulated doping profile has been analyzed and correlated with experimental results, in order to give indications for the correct interpretation of measured doping profile.**

***Index Terms* — CIGS, C-V, doping profiles, thin-film photovoltaics.**

I. Introduction

Capacitance-voltage (C-V) profiling is a standard technique for the determination of doping in semiconductor layers. In the ideal case, the net doping density is obtained measuring the depletion capacitance of an abrupt asymmetrical p-n junction [1].

However, in real devices the interpretation of C-V measurements is complicated by several factors, such as: i) the influence of shallow and deep defects [2]; ii) the deviation of junction doping from the abrupt unilateral profile; iii) the limits of the depletion approximation; iv) the non-uniformity of semiconductor doping [3]; in the case of CIGS cells, the presence of heterojunctions also contributes to the complexity.

The apparent doping profiles extracted from C-V plots in state-of-the-art CIGS solar cells exhibit a typical U-shape often reported in the literature [4], the minimum of which is generally taken as the true absorber doping density [2]. Moreover, the extracted apparent doping profiles are also temperature-dependent.

In this work we aim at interpreting this U-shape of the apparent doping profile extracted from C-V measurements by means of numerical simulations; in particular, we will examine the effect of: i) band-offsets at hetero-interfaces; ii) absorber, buffer, and window layer doping; iii) deep traps in the absorber.

II. Methods

In C-V measurements, an ac voltage perturbation is superimposed to the dc bias voltage, and the current response is measured to obtain the junction capacitance. The variation in junction capacitance with dc bias is then recorded. In the ideal case, using the depletion approximation, the charge density at the edge of depletion region $N_A(W)$ is given by:

$$N_A(W) = \frac{2}{qk_S\varepsilon_0}\frac{1}{A^2 d(1/C^2)/dV} \quad (1)$$

where W is width of the depletion region, A is the junction area, k_S is the semiconductor relative permittivity, ε_0 the permittivity of vacuum, and q is the electron charge. In a unilateral junction, the dominant capacitance response originates from the edge of the depletion region in the low-doped layer. The doping profiles extracted by (1) are usually plotted versus W, which is derived from the measured capacitance, C, as follows:

$$W(V) = \frac{k_S\varepsilon_0 A}{C(V)} \quad (2)$$

where both W and C are voltage dependent. However, because our analysis is focused on a hetero-structure, it is uncertain which relative permittivity value one should use in (2).

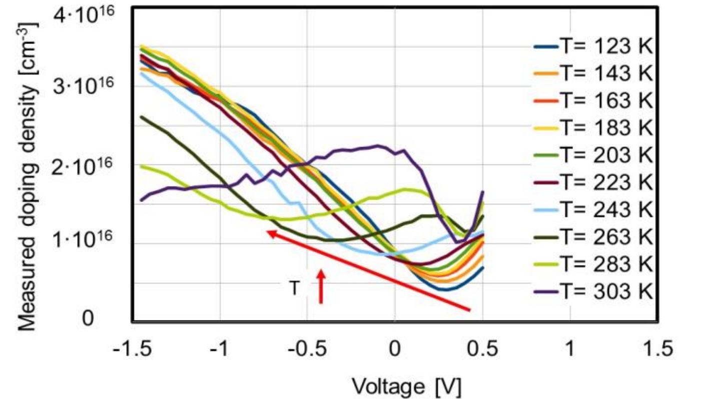

Fig. 1. Apparent doping density versus bias as extracted from C-V measurements according to (1).

For this reason, we plot the doping profiles extracted from the C-V curves versus the bias voltage, which is not affected by the relative permittivity value, k_S.

Capacitance-voltage curves of a CIGS solar cell were measured at different temperatures at EMPA; the corresponding apparent doping profiles versus bias voltage as extracted by (1) are reported in Fig. 1.

A. Simulations

We simulated the cell using the Synopsys Sentaurus-Tcad suite [5]. The cell behavior is described by the Poisson, electron and hole continuity, and drift-diffusion equations. Details about the structure of the simulated cell and the main used parameters are reported in Table I and in [6].

In the simulations shown hereafter, we first consider a defect–free cell and separately consider the effects of: A) CIGS/buffer conduction band offset ΔE_C(CdS/CIGS); B) CdS doping; C) intrinsic ZnO (i-ZnO) doping; D) CdS thickness; E) temperature.

Except for the cases where they are variable, we fix ΔE_C(CdS/CIGS) at 0.3 eV, the i-ZnO doping at $4 \cdot 10^{20}$ cm^{-3} (in order to simulate a case as close as possible to the ideal one-sided junction), the CdS doping and thickness at $4 \cdot 10^{16}$ cm^{-3} and 30 nm, and the temperature at 243 K.

In addition to that, we study the influence of CIGS acceptor and donor traps on the extracted doping profiles (as described in sub-section F).

The frequency of the small signal used to simulate the C-V method is 300 kHz in all simulations, well above the trap cut-off frequency.

TABLE I
MAIN PARAMETERS USED IN THE SIMULATIONS (T=300 K).

Material	ZnO(Al)	i-ZnO	CdS	CIGS
Eg [eV]	3.3	3.3	2.4	1.21
$\varepsilon/\varepsilon_0$	9	9	9	10
ΔEc [eV]	-0.2 (cliff)		Variable (spike)	
Nc 10^{18} [cm^{-3}]	2.27	2.27	2.27	0.677
Nv 10^{19} [cm^{-3}]	3.34	3.34	1.80	1.53
Thickness [nm]	200	80	variable	3000
Doping [cm^{-3}]	$4 \cdot 10^{20}$ (Donor)	variable (Donor)	variable (Donor)	$4 \cdot 10^{16}$ (Acceptor)
μ_e/μ_h [$cm^2/(V \cdot s)$]	100/25	100/25	100/25	100/25

III. RESULTS

A. Effects of the CdS/CIGS conduction band offset, ΔE_C(CdS/CIGS)

Fig. 2 shows that: (i) in spite of the presence of an hetero-structure, all curves converge to the real CIGS doping density ($4 \cdot 10^{16}$ cm^{-3}), provided that the voltage is negative enough, similar to [7]; (ii) the U-shape in the extracted doping profile, and the minimum appearing at bias voltage < 0.8 V (the sharp minimum at higher voltage is due to strong forward bias), are related with the existence of a conduction band offset at the CdS/CIGS interface; when ΔE_C(CdS/CIGS) = 0 eV (green curve of Fig. 2), the minimum disappears and the extracted doping profile follows that of a homo-junction.

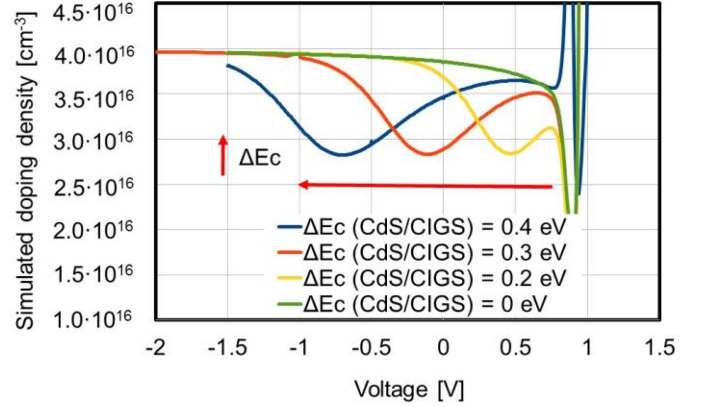

Fig. 2. Doping density versus bias as extracted from simulated C-V curves according to (1), for different values of CdS/CIGS conduction band offset, ΔEc(CdS/CIGS).

These simulations prove that the U-shape profile can appear even in the absence of traps or non-uniform absorber doping.

The observed behavior can be explained considering the electron channel arising at the CdS/CIGS interface when ΔE_C(CdS/CIGS) > 0 eV and enhanced by increasing band offset. In this situation, during the C-V measurements the modulated acceptor charge in the CIGS is balanced not only by the charge modulated in the n-doped layers, as in the classical homo-junction case, but also by the charge in this interface electron channel. We calculated the individual capacitance contributions of the ZnO and CdS layers, namely C_{ZnO} and C_{CdS}, and that of the electron channel at CdS/CIGS interface, $C_{ele\text{-}CdS/CIGS}$. The total cell capacitance, C_{tot}, has then been calculated as:

$$C_{tot} = C_{ZnO} + C_{CdS} + C_{ele\text{-}CdS/CIGS} \qquad (3)$$

and compared it with the simulated overall cell capacitance, C_{cell}. All capacitances are shown in Fig. 3 versus the applied voltage for the cases of ΔE_C(CdS/CIGS) = 0 and 0.3 eV, together with the corresponding doping profile extracted from C_{cell} using (1). Since C_{cell} and C_{tot} overlap independently of the value of ΔE_C(CdS/CIGS) and C_{ZnO} is always negligible, C_{CdS} and $C_{ele\text{-}CdS/CIGS}$ determine the shape of C_{cell}, thus controlling the value of the extracted doping profile. In the voltage range roughly corresponding to V > 0.7-0.8 V, the diode enters the diffusion regime where the hypotheses on which the C-V profiling technique is based loose validity: the N_A values extracted by (1) are no more related to the nominal CIGS doping.

As shown in Fig. 3a, in the case of ΔE_C(CdS/CIGS) = 0 eV, C_{CdS} dominates over $C_{ele\text{-}CdS/CIGS}$ up to large forward bias - where the whole model loses validity - so that $C_{cell} \approx C_{CdS}$, and the simulated doping profile resembles that predicted by the homo-junction theory. For ΔE_C(CdS/CIGS) = 0.3 eV (Fig. 3b), instead, C_{CdS} dominates only at low voltage ($V < V_{NA\text{-}MIN}$); at larger voltage ($V > V_{NA\text{-}MIN}$) $C_{ele\text{-}CdS/CIGS}$ becomes first

significant and then dominant: this change of regime determines the U-shape of the extracted doping profile, and its minimum, V_{NA-MIN}.

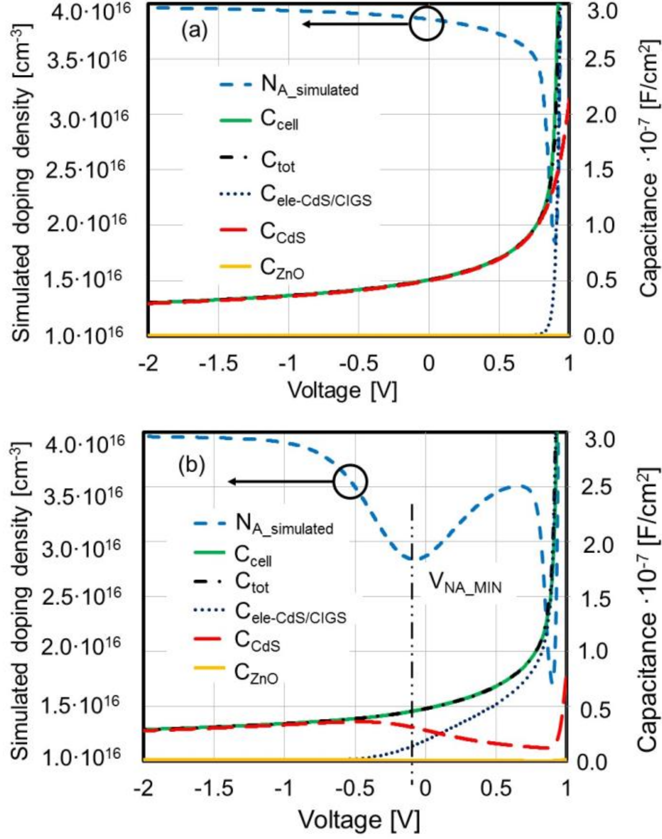

Fig. 3. Capacitance per unit area and doping density versus cell bias as extracted from simulated C-V curves according to (1). (a) ΔE_C(CdS/CIGS) = 0 eV; (b) ΔE_C(CdS/CIGS) = 0.3 eV.

B. Effects of CdS doping

Fig. 4 illustrates the effect of different doping density in the CdS layer. The shape of the apparent CIGS doping vs. voltage curve and the position and depth of the minimum are very sensitive to the CdS doping beyond 10^{17} cm^{-3}.

The more the simulated structure approaches the ideal unilateral junction case (high CdS doping), the shallower the minimum and the more negative the bias needed to obtain the match between extracted doping and nominal N_A, as for the case $N_{CdS} = 1 \cdot 10^{18}$ cm^{-3} where the nominal doping is reached for a very negative applied voltage (out of the scale of Fig. 4).

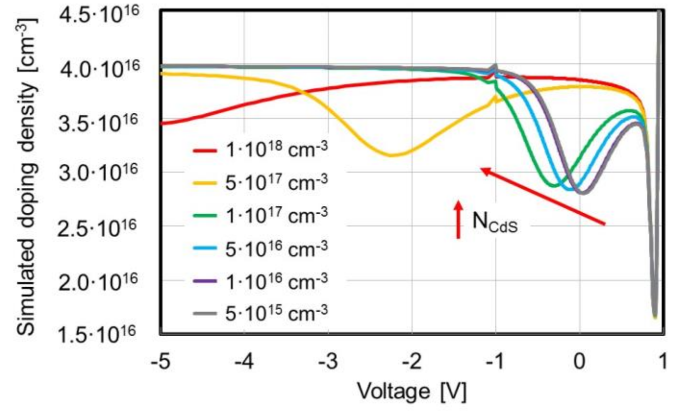

Fig. 4. Doping density versus cell bias as extracted from simulated C-V curves according to (1), for different values of CdS doping.

C. Effects of i-ZnO doping

The effect of i-ZnO doping is similar, as shown in Fig. 5. The larger the n-doping of the intrinsic portion of ZnO, the broader and shallower the minimum in the apparent doping vs. voltage plot.

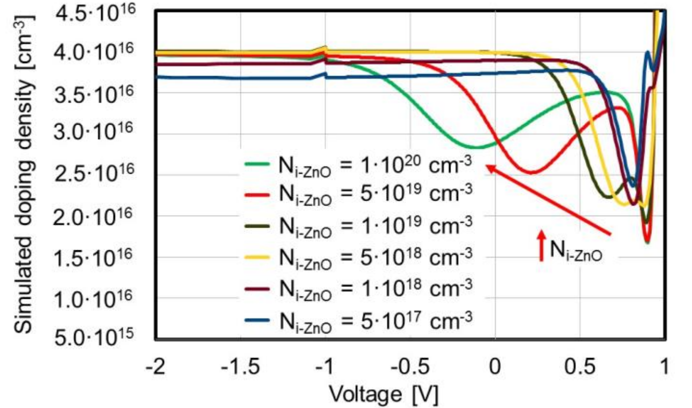

Fig. 5. Doping density versus cell bias as extracted from simulated C-V curves according to (1), for different values of intrinsic ZnO doping.

D. Effects of the CdS thickness

The CdS thickness also plays a role in shaping the doping profile extracted from the C-V, as shown in Fig. 6.

A thinner CdS, a heavier doping of CdS or i-ZnO, all cause the same effects: i) the shifting of V_{NA-MIN} (as defined in Fig. 3b) towards more negative values, and ii) the reduction of the depth of the minimum. The former is due to the increase of the electron density at CdS/CIGS interface that causes the related capacitance, $C_{ele-CdS/CIGS}$, to dominate over C_{CdS} for a wider bias range, so that V_{NA-MIN} is more negative. The latter is mainly related to the doping of the n-side of the junction (n-doped ZnO and CdS): the higher is the ionized donor charge, the closer the structure to the ideal one-sided junction case.

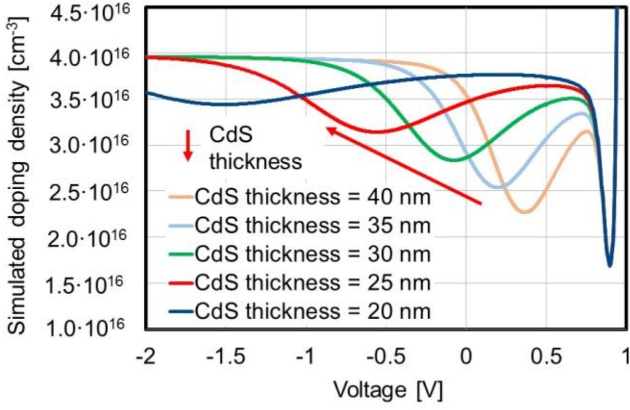

Fig. 6. Doping density versus cell bias as extracted from simulated C-V curves according to (1), for different values of CdS thickness.

E. Effects of temperature

The simulated effect of temperature on the extracted apparent doping profiles (Fig. 7) is similar to the measured one (Fig. 1), with a tendency of the minimum to become shallower and move toward more negative bias for higher temperatures.

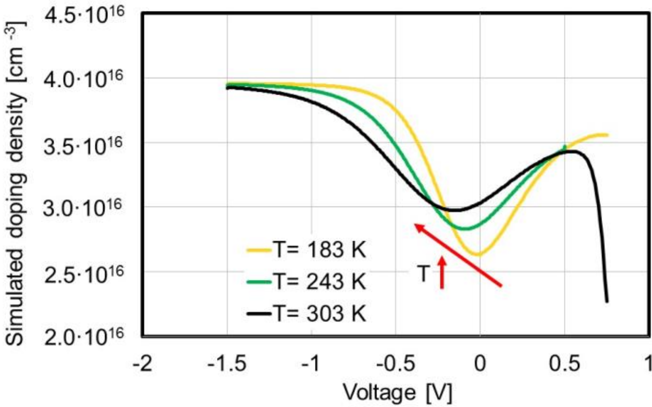

Fig. 7. Doping density versus cell bias as extracted from simulated C-V curves according to (1), for different temperatures.

F. Effects of bulk traps in the absorber

In this case, in order to compare the simulated cell parameters under illumination with the experimental ones, we revert to the typical CIGS solar cell stack (ZnO:Al/i-ZnO/n-CdS/p-CIGS) and fix the i-ZnO and CdS doping at 10^{17} cm^{-3} and $4{\cdot}10^{16}$ cm^{-3}, respectively. All the simulations with traps in the CIGS absorber are performed at 183 K.

We studied the effect of CIGS bulk traps on the extracted apparent doping profile N_A by inserting into the absorber trap centers with different concentration, activation energy and capture cross sections. Both acceptor and donor traps are considered, with density $N_{t\text{-}acc}$ and $N_{t\text{-}don}$. Traps are described by the classical Shockley-Read-Hall recombination model.

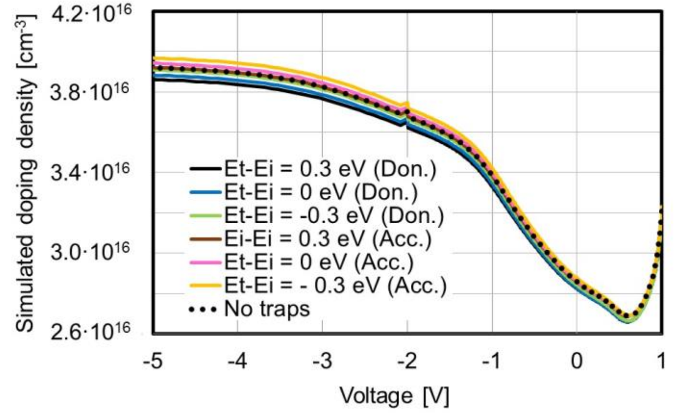

Fig. 8. Doping density versus cell bias as extracted from simulated C-V curves according to (1), for $N_{t\text{-}acc} = N_{t\text{-}don} = 6{\cdot}10^{14}$ cm^{-3}, $\sigma_n = \sigma_h = 10^{-15}$ cm^2, and different trap activation energies. T = 183 K.

As Fig. 8 illustrates, the presence of bulk traps in the CIGS with density $N_t = N_{t\text{-}acc} = N_{t\text{-}don} = 6{\cdot}10^{14}$ cm^{-3}, does not change the shape of the extracted apparent N_A profile, but the value reached at large negative voltage is slightly increased (decreased) by the contribution of ionized acceptor (donor) traps; this contribution also depends on the trap activation energy: it gets larger as the trap level moves away from the intrinsic Fermi level and gets shallower.

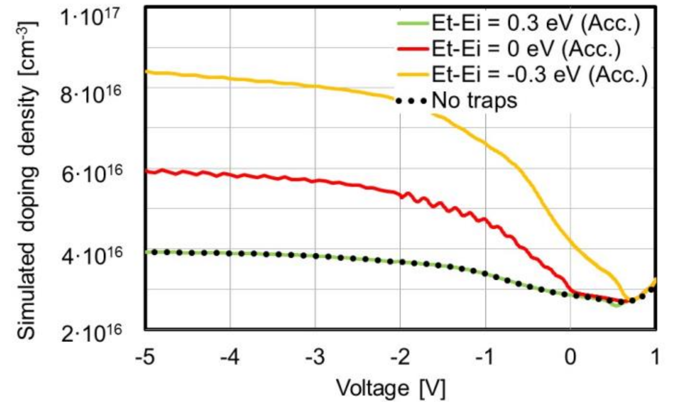

Fig. 9. Doping density versus cell bias as extracted from simulated C-V curves according to (1), for $N_{t\text{-}acc} = 6{\cdot}10^{16}$ cm^{-3}, $\sigma_n = \sigma_h = 10^{-17}$ cm^2, and different trap activation energies. T = 183 K.

The case where the deep acceptor trap density is increased to $N_{t\text{-}acc} = 6{\cdot}10^{16}$ cm^{-3}, which is larger than the CIGS doping, is shown in Fig. 9. When $E_t - E_i = -0.3$ eV, the acceptor traps are almost completely ionized and the apparent doping tends to $N_A + N_t = 10^{17}$ cm^{-3} for negative biases. On the other hand, the ionized acceptor traps density is negligible for $E_t - E_i = 0.3$ eV, and the extracted doping profile tends to $N_A = 4{\cdot}10^{16}$ cm^{-3}, i.e., the acceptor CIGS doping.

TABLE II
ACCEPTOR TRAP PARAMETERS USED IN SIMULATIONS, AND CORRESPONDING CELL PARAMETERS UNDER AM1.5G ILLUMINATION (T=300 K).

Et-Ei [eV]	σ_n=σ_p [cm^2]	N_t [cm^{-3}]	V_{OC} [V]	J_{SC} [mA/cm^2]	FF [%]	η
0.3	$1\cdot10^{-15}$	$6\cdot10^{14}$	0.79	33.4	76.9	20.3
	$1\cdot10^{-15}$	$6\cdot10^{16}$	0.72	28.3	55.6	11.3
	$1\cdot10^{-17}$	$6\cdot10^{16}$	0.79	33.3	72.9	19.1
0	$1\cdot10^{-15}$	$6\cdot10^{14}$	0.79	33.4	76.9	20.3
	$1\cdot10^{-15}$	$6\cdot10^{16}$	0.72	28.1	54.3	10.9
	$1\cdot10^{-17}$	$6\cdot10^{16}$	0.79	33.3	72.9	19.1
-0.3	$1\cdot10^{-15}$	$6\cdot10^{14}$	0.79	33.4	76.9	20.3
	$1\cdot10^{-15}$	$6\cdot10^{16}$	0.72	27.9	54.0	11.0
	$1\cdot10^{-17}$	$6\cdot10^{16}$	0.79	33.4	79.9	19.2

The presence of bulk acceptor traps might help explain the steep slope of the apparent doping profiles extracted from the measurements (see Fig. 1): these slopes cannot be reproduced in the simulations without traps in the CIGS. In order to verify if trap densities of this magnitude are compatible with the high efficiencies measured on these cells, the illuminated cell parameters are simulated and shown in Table II, for different values of trap parameters.

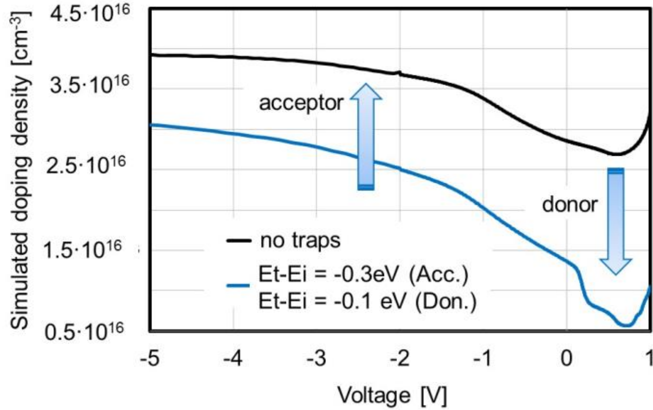

Fig. 10. Doping density versus cell bias as extracted from simulated C-V curves according to (1), for $N_{t\text{-}acc}$ = $1\cdot10^{16}$ cm^{-3} and $N_{t\text{-}don}$ = $3.5\cdot10^{15}$ cm^{-3}, σ_n=σ_h= 10^{-17} cm^2, and different trap activation energies. T = 183 K.

The simulations show that a concentration of deep acceptor traps higher than the doping can be present in high efficiency cell provided that their capture cross sections are sufficiently small, in the range of 10^{-17} cm^2: values like these have been reported in the literature [8].

The simultaneous presence of both acceptor and donor deep defects of proper density and energy can help shape the extracted doping profile and reproduce the measured doping excursion as shown in Fig.10, where the deep donor traps reduce the apparent doping profile mostly around the minimum at low positive bias, while acceptor traps have the opposite effect of increasing the doping, mainly at the negative biases.

VI. CONCLUSION

Our simulation study shows that the apparent doping profile extracted from the C-V plots is sensitive to several parameters, like n-doping densities (ZnO and CdS), buffer thickness, conduction band-offset at CdS/CIGS interface, and temperature.

The minimum of the apparent U-shaped doping profile always underestimates the actual doping of absorber, but it converges to that value when the negative bias is large enough.

We have shown here for the first time that the U-shape of the apparent doping profile extracted by the C-V plots is linked with the onset of an inverted channel at the CdS/CIGS interface, which is negligible at low bias, but tends to dominate the total junction capacitance when the voltage increases: the change of regime between these two situations corresponds with the minimum of the U-shape extracted doping profile.

Moreover, we have also proved that the contemporary presence of both acceptor and donor deep defects inside the CIGS can help explain the large excursion of apparent doping profile extracted by C-V measurements.

ACKNOWLEDGEMENT

This project has received funding from the *European Union's Horizon 2020 research and innovation programme* under grant agreement No 641004, project Sharc25.

REFERENCES

[1] D. K. Schroeder, *Semiconductor Material and Device Characterization*. Hoboken, New Jersey: John Wiley & Sons, Inc., 2006.

[2] M. Cwil, M. Igalson, P. Zabierowski, and S. Siebentritt, "Charge and doping distributions by capacitance profiling in Cu(In,Ga)Se2", *Journal of Applied Physics*, vol. 103, pp. 063701-1 - 063701-9 , 2008.

[3] C. P. Wu, E. C. Douglas, C. W. Muller, "Limitations of the CV technique for Ion-Implanted Profiles", *IEEE Transactions on Electron Devices*, vol. ED-22, no. 6, pp. 319-329 1975.

[4] Michał Ćwil, M. Igalson, P. Zabierowski, C. A. Kaufmann, A. Neisser, "Capacitance profiling in the CIGS solar cells", *Thin Solid Films*, vol. 515, pp. 6229–6232, 2007.

[5] http://www.synopsys.com/Tools/TCAD.

[6] G. Sozzi, D. Pignoloni, R. Menozzi, F. Pianezzi, P. Reinhard, B. Bissig, S. Buecheler, A. N. Tiwari, "Designing CIGS solar cells with front-side point contacts", *Proc. 42th IEEE Photovoltaic Specialists Conference (PVSC)*, 2015; doi: 10.1109/PVSC.2015.7355691.

[7] M. Maciaszek and P. Zabierowski, "The Influence of the n-Side Doping on Metastable Defect Concentrations in Cu(In,Ga)Se2 Evaluated From Space Charge Profiles", *IEEE Journal of Photovoltaics*, vol.5, no. 5, pp. 1454-1461, 2015.

[8] L.L. Kerr, Sheng S. Li, S.W. Johnston, T.J. Anderson, O.D. Crisalle, W.K. Kim, J. Abushama, R.N. Noufi, "Investigation of defect properties in Cu(In,Ga)Se2 solar cells by deep-level transient spectroscopy", *Solid-State Electronics*, vol. 48, pp-1579–1586, 2004.